Check for updates

Received: 15 August 2023 | Revised: 9 October 2023 | Accepted: 11 October 2023

DOI: 10.1002/pen.26536

RESEARCH ARTICLE

POLYMER ENGINEERING AND SCIENCE WILEY

Effects of the injection molding processing settings on the phase morphology and mechanical anisotropy of thermoplastic vulcanizates

Noah Mentges | **Hakan Çelik** | **Rainer Dahlmann** | **Christian Hopmann**

Institute for Plastics Processing (IKV) at RWTH Aachen University, Aachen, Germany

Correspondence
Noah Mentges, Institute for Plastics Processing (IKV) at RWTH Aachen University, Aachen, Germany.
Email: noah.mentges@ikv.rwth-aachen.de

Funding information
Deutsche Forschungsgemeinschaft, Grant/Award Number: 448100263

Abstract

Thermoplastic vulcanizates show significant anisotropic mechanical properties when processed to components via injection molding. This effect is related to a process-dependent distortion of the incorporated elastomer particles in high-shear regions during the injection phase. In a plate geometry, the elastomer particles in the shear regions are oriented and deformed in the flow direction. However, the ongoing distortion processes and the influencing factors of the process parameters on the resulting phase morphology and mechanical response are not entirely understood. Therefore, in this study, the effect of the injection molding machine settings for the production of a plate component on the local phase morphology and mechanical anisotropy is investigated. The investigations are conducted on two commercial material grades with different Shore-A hardness 30 and 90. A significant inverse effect of the injection volume flow rate on the particle distortion and anisotropy is found. Increasing the volume flow rate results in a reduction of the anisotropy. This is counterintuitive from the experience of other materials with process-dependent anisotropy. Also, a significant influence of the process on the overall stiffness of the compounds is observed.

Highlights

- Sturcture–property relation for phase morphology in thermoplastic vulcanizates
- Quantitative microstructure analysis in injection molded plates
- Macroscopic analysis of anisotropic mechanical response under uniaxial loading
- Effect analysis of injection molding parameters on the mechanical anisotropy
- Additional effects of process settings on overall stiffness of the material

KEYWORDS

anisotropy, phase morphology, thermoplastic vulcanizates

This is an open access article under the terms of the Creative Commons Attribution-NonCommercial License, which permits use, distribution and reproduction in any medium, provided the original work is properly cited and is not used for commercial purposes.
© 2023 Institute for Plastics Processing at RWTH Aachen. *Polymer Engineering & Science* published by Wiley Periodicals LLC on behalf of Society of Plastics Engineers.

1 | INTRODUCTION

Thermoplastic vulcanizates (TPV) are a subcategory of the thermoplastic elastomer (TPE) material class. TPV are polymer blends consisting of vulcanized elastomer particles embedded in a thermoplastic matrix material.[1–4] Usually, elastomer volume contents are in the range of 40% for TPV with high Shore hardness and 90% for soft TPV.[5] The range of hardness for TPV is usually between 30 ShoreA and 40 ShoreD. The mechanical behavior of TPV materials is comparable to that of rubber materials. However, TPVs generally show higher plastic deformation under unloading and stress softening on cyclic reloading of the material.[1] This is due to the yielding of the thermoplastic component under high stretches. Hence, it is shown that the macroscopic mechanical response of the material is governed by the local phase morphology. Micromechanical investigations by Boyce, Socrate et al. show that the microscopic configuration of the material affects the mechanical response under loading, unloading, and reloading.[3,6,7] In correlation with the elastomer volume content, the material response gradually shifts from a thermoplastic behavior to a rubberlike response.[6] Recent research in the field of TPV focuses on the development of improved compounds for special use cases such as improving fire resistance and strength with the addition of nano-particles[8] or regarding structure–property relation with respect to the size distribution and agglomeration mechanisms of the elastomer phase.[9] However, in most cases, the significant influence of the injection molding process on the morphology development and its corresponding effects on physical properties of the compound are neglected.

Most TPV materials are processed in the injection molding process. High shear flow rates during the injection phase of the process lead to distortions of the elastomer particles, especially in the areas close to the cavity walls.[10] Additionally, the high cooling rates in these areas lead to a fixation of the distorted particles, affecting the TPV's local microscopic configuration and resulting in a preferential direction.[10] The shear rates are negligible in the center of the flow cross-section. Hence, the elastomer particles remain in their undistorted state. In more complex flow regions, at redirections, or splitting of the flow channel, other phenomena occur that influence the distortion of the elastomer particles and, thus, the local micromechanical configuration of the TPV.

Uniaxial tension tests have shown that these local configurations lead to strong anisotropies in the material.[3,10,11] On an injection molded0 plate, stress reductions of the uniaxial response perpendicular to the flow directions of around 40% have been measured compared with the response in the parallel direction of flow at equivalent stretch levels.[11] The local microscopic configuration of the TPV is strongly influenced by the material composition. Harder TPVs show a lower anisotropy than softer materials due to the varying volume contents of elastomers.[3] Nevertheless, processing parameters influence the particles' distortion state, as shown in Reference 3. In a recent publication by Burgoa et al.,[12] the anisotropic nature of injection molded TPV has been confirmed.

For a given cavity, the local process parameters (shear velocity, melt temperature, and pressure) are directly affected by the injection molding machine parameters. Hence, the effect of fundamental machine parameters, cavity cooleant temperature, injection temperature, and injection volume flow rate, on the anisotropic mechanical response of TPV is investigated in this work. The tests are performed on two different TPV in order to investigate the difference in the effect analysis considering different compositions of the thermoplastic and elastomeric components. Hence, a soft TPV with 30 ShA and a relatively hard component with 90 ShA hardness are chosen. Considering the injection molding parameters, a fully factorial test plan is performed on the three fundamental machine parameters cavity temperature, melt temperature, and injection volume flow rate. Uniaxial, quasi-static, cyclic tension tests are performed on specimens extracted from an injection molded plate. Transmission microscopy images are obtained and investigated for the TPV material with 90 ShA to quantify the local phase morphology in the injection molded plate. The obtained images are quantitatively analyzed using an automated image processing routine regarding the plate-thickness-dependent particle distortion and orientation state.

2 | FORMATION OF ORIENTATIONS IN TPV DURING INJECTION MOLDING

The process of orientation formation in TPV is driven by the local shear flow in the injection molding process. In regions of high shear rates, the melt is subjected to high shear stresses. These lead to a distortion of the elastomer particles during the filling process. The deformation of the elastomer particles results in the increase of a viscoelastic potential. This potential is reduced as a function of time when the elastomer particles retract when the shear flow is stopped. However, due to the high cooling rates in injection molding, the particle distortions in the material cannot be completely recovered before the melt solidifies. Consequently, a portion of the viscoelastic potential is preserved. Especially, the solidification of the melt in the proximity of the cavity wall leads to a locking of the

15482634, 0, Downloaded from https://4spepublications.onlinelibrary.wiley.com/doi/10.1002/pen.26536 by Rwth Aachen Hochschulbibliothe, Wiley Online Library on [02/11/2023]. See the Terms and Conditions (https://onlinelibrary.wiley.com/terms-and-conditions) on Wiley Online Library for rules of use; OA articles are governed by the applicable Creative Commons License

deformed particles. Further into the cavity center, this deformation can recover for a longer period until the melt has solidified. The described mechanisms are illustrated in a figure provided in the supplementary material.

Resulting from these mechanisms, the phase morphology of TPV over a plate cross-section can be divided in three distinct zones.[3] The shear zone close to the cavity walls is defined by high distortion and orientation of the elastomer particles. In the cavity center a core zone is found with low particle distortion. Thirdly, an intermediate transition zone is defined in between the two extremes.

To understand the effect of elastomer particle orientations in TPV on the anisotropic mechanical response, the local deformation mechanisms under quasi-static loading are described briefly. Soliman et al. proposed an according model in References 13,14 for a TPV in quasi-isotropic configuration. They described the morphology of TPV with three distinct regions. The first region is the elastomer inclusions. Secondly, there is the thermoplast matrx which is devided in two subregions, first, the thin thermoplastic ligaments between two elastomer inclusions and, second, the larger volumed regions in between three or more inclusions. All three different regions contribute differently to the macroscopic deformation. The soft elastomer particles contribute to high deformation and a low-stress response. The thin thermoplastic ligaments act as strain bridges between the elastomer particles and are, therefore, also subjected to large strains. In comparison, the higher volume thermoplastic regions do not contribute to the macroscopic deformation significantly. Soliman et al. used molecular strain measurements with infrared scattering to support their theory.

It is assumed that the much stiffer thermoplastic component contributes significantly to the macroscopic stress response of the TPV. Consequently, when adding a particle distortion to the model, also the thermoplastic ligaments orient themselves in a preferential direction. Hence, an anisotropic macroscopic stress response of the TPV can not solely be attributed to the distortion- and orientation-state of the elastomer particles. The effect of the orientation of significantly stiffer thermoplastic ligaments on the anisotropic nature is expected to be even more decisive.

3 | MATERIALS AND METHODS

3.1 | Materials

Two industrial TPV compounds are investigated for the study. One soft TPV with Shore A hardness of 30 with the trade name Alfater XL A30I 4GP0000 is used. The other compound is a hard TPV with a Shore A hardness of 90, namely Alfater XL A90I 4GP0000. They are provided by the MOCOM Compound GmbH & Co. KG, Hamburg, Germany.

The blends consist of polypropylene (PP) as a thermoplastic matrix and ethylene propylene diene rubber (EPDM) as an elastomeric material. In both compounds, a peroxidic cross-linking system is used for vulcanizing the rubber phase in the dynamic vulcanization process. It should be mentioned that the peroxidic cross-linking agent not only affects the elastomer phase in the vulcanization process but also attacks the PP chains. This affects the mechanical properties of the PP phase in dependence of the content of cross-linking agent and, hence indirectly, the elastomer content in the compound.[15,16] The two investigated materials will be referred to as TPV ShA30 and TPV ShA90 in relation to the respective Shore-hardness.

3.2 | Processing and specimen extraction

Plates with the dimensions $170 \times 170 \times 2$ mm are produced in the injection molding process for both materials. The plates are manufactured on a KM 160–1000 CX injection molding machine from KraussMaffei Group GmbH, Munich, Germany. The machine settings for the production of the TPV test plates are summarized in Table 1.

The parameters cavity temperature, melt temperature at injection, and injection volume flow rate have been varied in a fully factorial test plan to determine the effect of the processing parameters on the mechanical response. These parameters are chosen since they are expected to have the most significant effect on the local flow conditions in the cavity and, hence, the microscopic configuration of the TPV.

The varied machine parameters are chosen according to the material data sheets.[17,18] In the following, the different machine parameter sets will be referred to with the corresponding indices L, M, H (referenced in Table 1) in the following order: Cavity temperature, melt temperature, and injection volume flow rate. Exemplarily, the process parameter set LHH refers to a cavity temperature of 30°C, a melt temperature of 220°C, and a volume flow rate of 300 cm^3/s.

For mechanical testing, five S2 tensile test specimens in reference to DIN 53504[19] are extracted from each test plate via stamping. The specimens are taken considering the extraction angle in reference to the flow direction during cavity filling. Three different orientations are considered, namely 0°, 45°, and 90°. Plate geometry and the extraction regions can be obtained from the supplementary files. Additionally, smaller specimens are extracted for microscopic investigations of the phase morphology. The cross-sections parallel to the direction of flow are analyzed to identify the particle distortion.

15482634, 0, Downloaded from https://4spepublications.onlinelibrary.wiley.com/doi/10.1002/pen.26536 by Rwth Aachen Hochschulbibliothe, Wiley Online Library on [02/11/2023]. See the Terms and Conditions (https://onlinelibrary.wiley.com/terms-and-conditions) on Wiley Online Library for rules of use; OA articles are governed by the applicable Creative Commons License

Processing parameter	Symbol	Unit	Value		
			L	M	H
Cavity temperature	T_C	°C	30	45	60
Melt temperature	T_M	°C	195	208	220
Injection volume flow rate	$\dot{V}$	cm^3/s	80	190	300
Maximum injection pressure		bar	800		
Holding pressure		bar	600		
Holding pressure time		s	15		
Dosing volume		cm^3	145		
Dosing circumferential speed		mm/s	288		
Decompression volume after dosing		cm^3	25		
Switch-over volume		cm^3	50		
Cooling time		s	10		

TABLE 1 Injection molding machine settings for the production of TPV specimen plates.

3.3 | Microscopic investigations

For investigation of the phase morphology of the TPV, specimens are extracted and inspected on the cross-sectional area parallel to the flow direction. The specimens are taken from the injection molded plates on the left side of the centered tensile test specimen with 0° extraction orientation. For examination in the transmitted light microscope, thin sections with a thickness of approximately 12 μm are prepared using a microtome. The cuts were produced at room temperature. Microscopy images have been obtained using transmitted light microscopy obtained with a microscope by Leica Microsystems GmbH, Wetzlar, Germany. A coordinate system is introduced with the x-axis parallel to the flow direction. The y-axis is in the plate thickness direction. This coordinate system is used consistently throughout this publication to simplify the interpretation of the particle orientation state through the thickness.

Microscopic investigations are only performed on the TPV ShA90 component. For the softer TPV ShA30, the available methods are unsuitable for the specimen preparation of sufficiently accurate surface qualities. Additionally, the black coloring of the thermoplastic phase in the TPV ShA90 allows for a quantitative analysis of the phase morphology with respect to the local particle distortion using the phase contrast and automated image processing routines.

3.4 | Quantitative analysis of the phase morphology

For a quantitative investigation of the local elastomer particle distortion, the microscopy images of the specimen plate cross-sections are processed using the python implementation of OpenCV. For this, the image is converted into a gray-scale image and processed with a Gauss filter for better edge detection. The image is then converted into a binary image using the Otsu thresholding method.[20] From these, the contours in the binary image are extracted and best-fit ellipses are applied on the inclusion contours. The extracted ellipse shapes are evaluated using the center coordinates, major and minor axes, and the angle of the major axis with respect to the horizontal X-coordinate. Figure 1 shows a microscopy image of a TPV ShA90 cut with the detected ellipses added to the highlighted region in the neighboring graphics. It should be noted that the analyzed images are cropped from the original image to eliminate any boundary effects induced by the cutting procedure. Consequently, some information of the phase morphology from the cross-section borders is not considered in the analysis. Also, it should be mentioned that there are some errors in the automatic edge detection algorithm. For example, in the upper right corner, where an obvious cluster of shapes is considered as a single, large inclusion. It is noteworthy that the distortion and orientation state of an elastomer particle is reduced to a two-dimensional representation of the geometry. A reliable statement about the three-dimensional distortion state of the elastomer particles cannot be made from these images. Hence, the resulting morphology description can be only a qualitative estimate and should not be considered as a realistic description of the phase morphology.

The generated ellipse parameters can be used to calculate an orientation tensor using the equivalent description of a second-order fiber orientation distribution tensor $\boldsymbol{A}$ for discontinuously fiber-reinforced

15482634, 0, Downloaded from https://4spepublications.onlinelibrary.wiley.com/doi/10.1002/pen.26536 by Rwth Aachen Hochschulbibliothe, Wiley Online Library on [02/11/2023]. See the Terms and Conditions (https://onlinelibrary.wiley.com/terms-and-conditions) on Wiley Online Library for rules of use; OA articles are governed by the applicable Creative Commons License

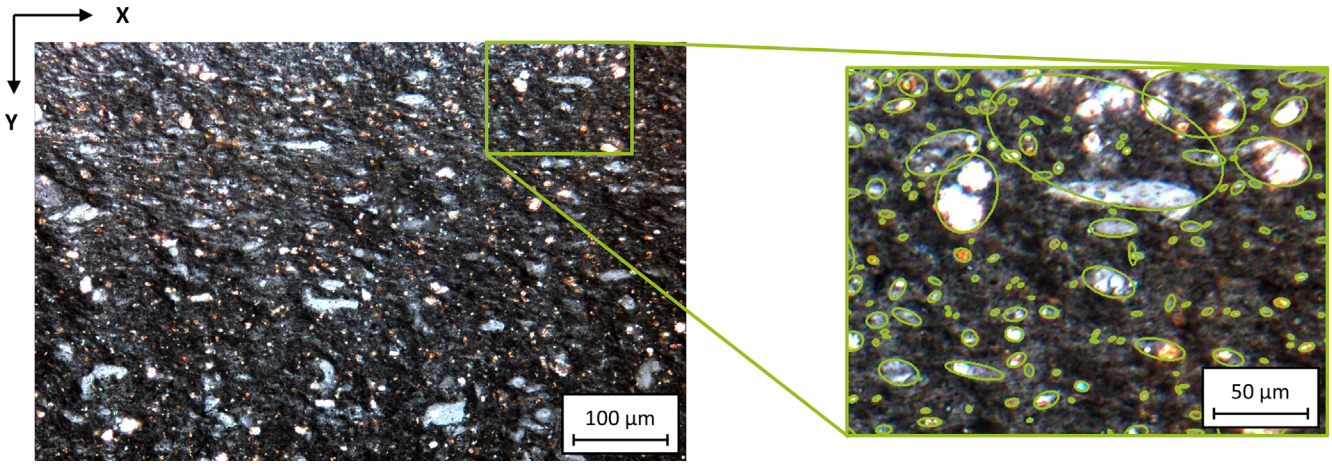


FIGURE 1 Exemplary transmission light microscopy image with detected ellipsoids from the automated image processing algorithm for quantitative analysis of the TPV phase morphology of a specimen from the LLL parameter set (see Table 1).

composites following Advani and Tucker.[21] In the case of fiber-reinforced composites, $\boldsymbol{A}$ represents the statistical distribution $\Psi(\boldsymbol{p})$ of fiber orientations $\boldsymbol{p}$, defined in the two-dimensional state by

$$\boldsymbol{A} = \oint \Psi(\phi)\ \boldsymbol{p}(\phi) \otimes \boldsymbol{p}(\phi)\ d\phi, \tag{1}$$

where $\otimes$ represents the dyadic tensor product and ϕ the angle relative to one axis of the coordinate system. $\boldsymbol{A}$ is a symmetric, positive definite structural tensor and $A_{ii} = 1$. The tensor can be diagonalized using coordinate transformation. Additionally, $\boldsymbol{A}$ comes with important properties which make it suitable for describing the orientation and distortion state of elastomer inclusions in TPV. First, the orientation distribution tensor can be interpreted as an elliptical shape with major and minor axes equal to the diagonal entries of $\boldsymbol{A}$ in its diagonalized form. Similar interpretations of a structure tensor have been first used by Basser and Pierparoli for the visualization of diffusivity tensors in brain tissues.[22] An idealization of the elastomer inclusion shape as an ellipse i with respective major and minor axes a_i and b_i and an orientation angle θ_i allows for a direct application of the distortion state of the inclusion to an orientation tensor $\boldsymbol{A}_i$, with

$$\boldsymbol{A}_i = \frac{1}{a_i + b_i} \boldsymbol{R}^T(\theta_i)\, diag(a_i, b_i)\, \boldsymbol{R}(\theta_i), \tag{2}$$

$$\boldsymbol{R}(\theta_i) = \begin{pmatrix} \cos\theta_i & \sin\theta_i \\ -\sin\theta_i & \cos\theta_i \end{pmatrix}. \tag{3}$$

A geometric depiction of the presented parameters of an ellipsoid is given in the supplementary material. Also, according to Equation (1), the orientation distribution tensor is constructed based on an averaging method of single fiber orientation states. Hence, the averaged orientation state $\boldsymbol{A}$ of multiple elastomer inclusions i can be obtained with an individual weighting regarding the respective cross-section area of the ellipse, with

$$\boldsymbol{A} = \frac{\sum_i a_i b_i \boldsymbol{A}_i}{\sum_i (a_i b_i)}. \tag{4}$$

The analogy of using the orientation distribution tensor is additionally supported by the possibility of describing the local phase morphology of both materials with the same mathematical formulation. Also, the formation of this phase morphology in the injection molding process is based on similar mechanisms driven by the shear conditions. With this, existing methods for obtaining the local phase morphology of discontinuously reinforced composites, such as proposed by Folgar and Tucker,[23] can be used and extended for the application on TPV morphology predictions. An averaged orientation tensor $\boldsymbol{A}$ could be interpreted as averaged inclusion with an elliptic shape for the investigated region. Consequently, the entry of the orientation tensor A_{XX} could be interpreted as the averaged orientation degree of the averaged ellipse in X-direction. In analogy A_{YY} can be interpreted as orientation degree in the Y-direction. A_{XY} is a measure of the rotation of the Ellipse in the XY-plane. An ideal circle would be represented by the orientation tensor $\boldsymbol{A} = diag(0.5, 0.5)$.

To describe the thickness-dependent orientation state of the injection molded TPV cross-section, a rolling average orientation state is obtained with respect to the inclusion center coordinate in the thickness direction. For a given center coordinate y, all detected ellipses within a

15482634, 0, Downloaded from https://4spepublications.onlinelibrary.wiley.com/doi/10.1002/pen.26536 by Rwth Aachen Hochschulbibliothe, Wiley Online Library on [02/11/2023]. See the Terms and Conditions (https://onlinelibrary.wiley.com/terms-and-conditions) on Wiley Online Library for rules of use; OA articles are governed by the applicable Creative Commons License

certain thickness range h are included in the calculation of the average orientation state following Equation (4).

As the derived orientation tensor describes the average distortion and orientation state of the elastomer particles, the formulation is not completely capable of describing all relevant orientations as described in Section 2. However, it seems reasonable that a direct correlation between the elastomer particle distortion and the orientation distribution of the thin thermoplastic ligaments can be found. Further investigation in this field must be conducted.

3.5 | Mechanical testing

The cyclic, quasi-static, mechanical tests are performed at room temperature on a universal testing machine type Z10 and Z100 from ZwickRoell GmbH & Co. KG, Ulm, Germany. Pneumatic grips are used for clamping the specimen. Load cells with maximum forces of 1 kN are used. The test is displacement controlled. For optical strain measuring, a camera of type Marlin F-146 B/C by Allied Vision Technologies GmbH, Stadtroda, Germany is used in combination with the evaluation software VicGauge by Limess Messtechnik & Software GmbH, Krefeld, Germany. The captured parallel strain is chosen to determine the switch point for cyclic testing by the control unit of the testing machine. The specimens are tested with a constant rate of 50 mm/min up to three stretch levels λ of 1.1, 1.2, and 1.3 and then unloaded to 0 N with the same deformation rate. Ten loading cycles are applied before the next stretch level is approached. For each test configuration, specimens from three injection molded plates are tested, resulting in 15 tests in total for each process parameter set and orientation.

4 | RESULTS

4.1 | Qualitative analysis of the phase morphology

To evaluate the effect of the local flow conditions resulting from the injection molding process on the local phase morphology, microscopy images of the entire plate cross-section are investigated first. Figure 2 presents three images of cross-sections of the injection molded plates from the TPV ShA90 material for the most extreme injection molding.

Production settings, LLL (a), MMM (b), and HHH (c). For these machine settings, the most significant effect regarding the mechanical anisotropy of the TPV and, consequently, on the local phase morphology is expected. The direction of flow in these images is horizontal.

In all images, most of the material is black due to the black coloring of the compound. However, small inclusions can be found which are translucent. These inclusions have diameters of up to 50 μm. It is considered that the translucent inclusions represent some of the

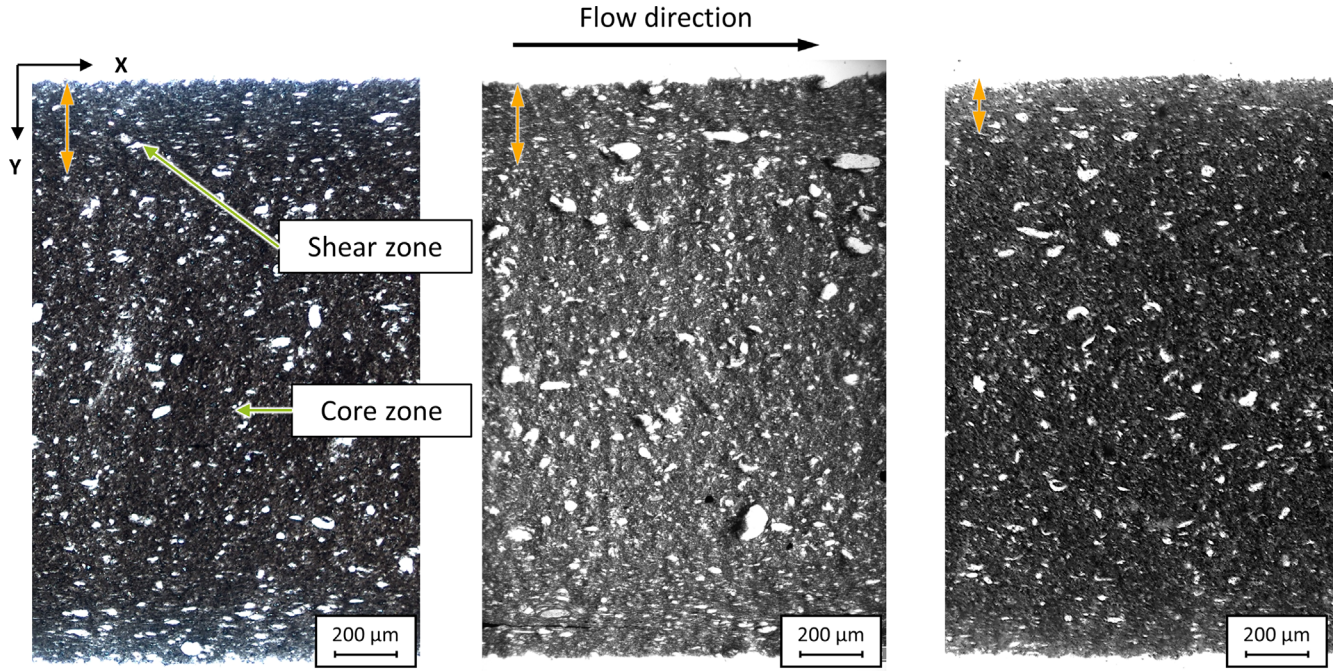


FIGURE 2 Light microscopy images of the cross-section of the TPV ShA90 for the most deviating machine parameter settings LLL (A), MMM (B), and HHH (C).

15482634, 0, Downloaded from https://4spepublications.onlinelibrary.wiley.com/doi/10.1002/pen.26536 by Rwth Aachen Hochschulbibliothe, Wiley Online Library on [02/11/2023]. See the Terms and Conditions (https://onlinelibrary.wiley.com/terms-and-conditions) on Wiley Online Library for rules of use; OA articles are governed by the applicable Creative Commons License

elastomer phases. This is supported by the fact that, in TPV, the elastomer phase is a discontinuous phase surrounded by the thermoplastic matrix. However, much smaller inclusions are expected to be found up to the size of 1 μm. These inclusions may not be represented in these images for two reasons. First, the resolution of the image is not fine enough. Secondly, the thickness of the cut is higher than the inclusion dimensions.

All three images show the characteristic three-layer structure of an injection molded plate. A shear zone can be identified in the cross-sections' outer regions. It is characterized by the highly distorted particles oriented in the direction of flow. In the center of the flow channel, a lower orientation state is found, resulting from the lower shear velocities in this region during the injection molding process. Comparing the three images with each other, different thicknesses of the shear zone are identified. These are indicated by the orange markers in Figure 2. The LLL parameter set specimen shows the highest thickness of the shear zone, whereas the HHH specimen shows the lowest thickness of the shear zone. Manual measurements of the shear zone thickness result in approximately 290, 270, and 140 µm for the LLL, MMM, and HHH cases, respectively. The measured thicknesses are indicated by the orange arrows in Figure 2. It should be noted that the transition beeween shear- and core-zone is gradual. Hence, finding exact measurements for the zone borders is subjective.

4.2 | Quantitative analysis of the microscopy images

For a better quantification of the local phase morphology, the inclusion shapes of the microscopy images are analyzed according to Section 3.4. First, the full cross-sectional images presented in Figure 2 are investigated. Subsequently, to obtain a better understanding of the highly oriented particles in the shear-zone, images with higher resolution of these regions are analyzed.

For the investigation of the ellipse distortion state along the entire specimen cross-section, the rolling average orientation tensor entries are plotted in dependence of the *Y*-coordinate in the image for the three investigated machine parameter sets LLL, MMM, and HHH in Figure 3. For this analysis, the inclusion zone for the rolling average is set to 100 µm. All three graphs show a similar trend of the orientation state development over the plate thickness. It starts with a region with a predominant orientation in the *X*-direction. This section gradually decreases to a nearly isotropic state in the center of the plate. On the opposite side of the plate, the orientation state in *X*-direction, A_{XX}, increases symmetrically. This coincides with the three-layered structure already observed in the microscopy images. The off-diagonal entry of the orientation tensor is close to 0 for all cases and indicates a good correlation of the coordinate system of the microscopy images with the global plate coordinate system as well as a low deviation of the averaged orientation state from the *X*-axis. Since the *XY*-tensor, A_{XY}, entry is relatively low for all three cases and, therefore, neglected in the following.

In comparison, Figure 3A for the LLL parameter set shows the highest orientation degrees in the shear zones. Also, the relative thickness of the shear zone is the largest in comparison with the other two parameter settings. Additionally, the decline of the transition region to the isotropic core zone is more significant, especially in comparison with the HHH parameter set. Opposite to this, the progression of the orientation state for the HHH parameter set contains much lower gradients in the orientation degree. However, it is noted that the core zone is fully isotropic. The MMM parameter set gives an intermediate version of the progressions of the orientation state.

For a deeper understanding of the orientation state in the shear zone, higher-resolution images of the region have been obtained and analyzed as before. Exemplary images of the according regions are depicted in Figure 4. In order to have a better statistical coverage, three selected images are incorporated into the automated orientation degree analysis. For the rolling average window, a thickness of 30 μm is chosen for this analysis. The resulting progressions of the orientation tensor are presented in Figure 5 for each parameter set.

The three depicted progressions of the orientation state show relatively similar values with regard to the *Y*-coordinate of the image. However, as in the previous investigations, the specimen with the LLL parameter set in Figure 5A shows the highest orientation state slightly under the plate surface at around 150 μm. Generally, for the LLL and MMM Figure 5B specimen, an incline of the orientation state at low thicknesses is observed. The orientation state reaches a maximum before it reduces with higher *Y*-values. The orientation state from the HHH Figure 5C specimen has its maximum at $Y = 0$ μm. It is also noticed that the maximum orientation state for the HHH parameter set is higher than the maximum orientation state for the MMM parameter set.

In conclusion, it is observed that the orientation state of the microscopy images represents the typical three-layered structure of the injection molded plate, starting with a shear zone with highly oriented particles within the direction of flow, a transition to the core zone, where a rather isotropic orientation state is found. It should be noted that for fiber-reinforced composites, a transversely oriented layer is found in the core zone due to the swell flow condition resulting from the

15482634, 0, Downloaded from https://4spepublications.onlinelibrary.wiley.com/doi/10.1002/pen.26536 by Rwth Aachen Hochschulbibliothe, Wiley Online Library on [02/11/2023]. See the Terms and Conditions (https://onlinelibrary.wiley.com/terms-and-conditions) on Wiley Online Library for rules of use; OA articles are governed by the applicable Creative Commons License

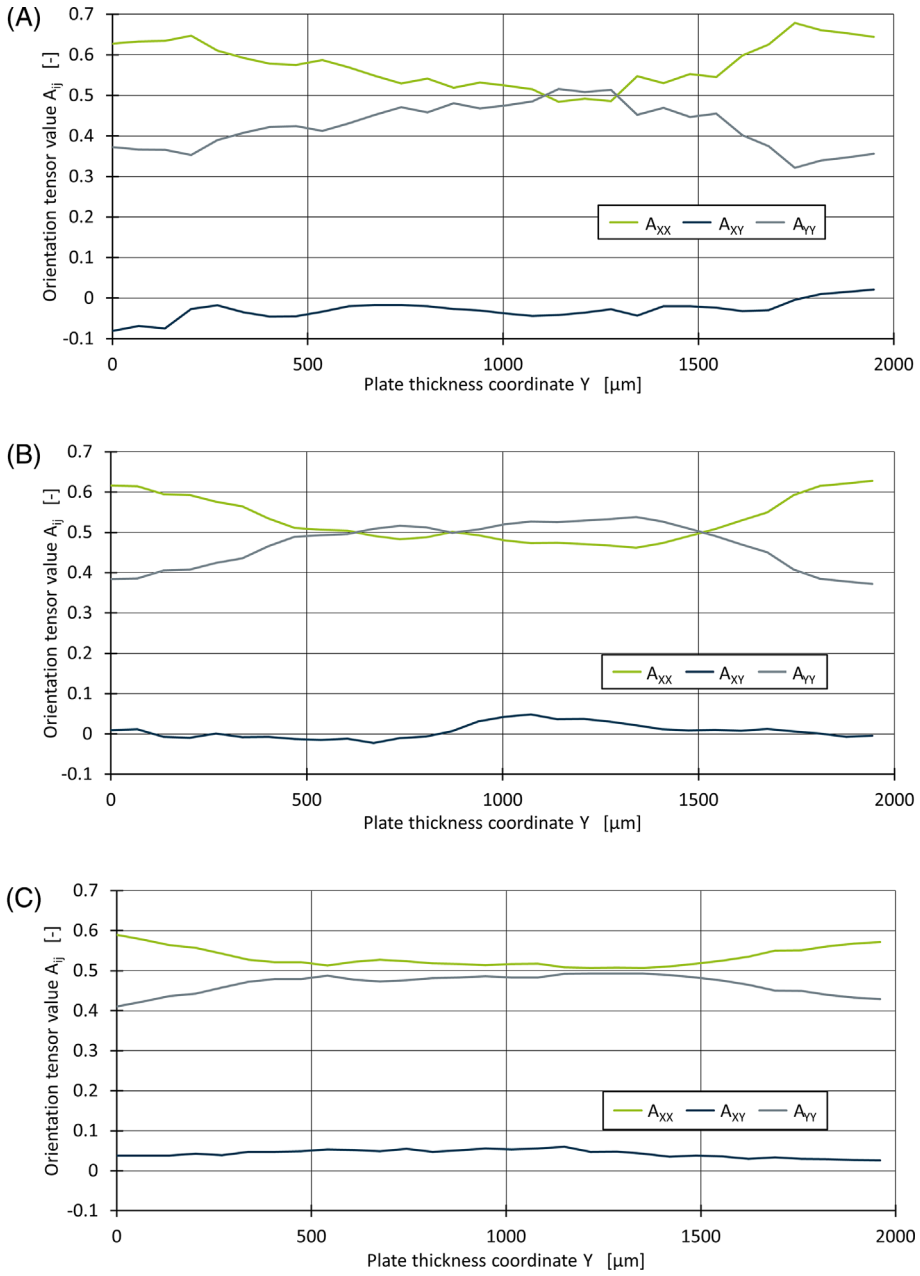


FIGURE 3 Rolling average particle orientation degree from microscopy images for the entire plate cross-section produced with the respective machine parameter sets LLL (A), MMM (B), and HHH (C).

injection sprue. To confirm such an orientation state in the TPV, investigations under the microscope perpendicular to the direction of flow should be conducted additionally.

4.3 | Mechanical testing

The resulting force strain data from the uniaxial tension tests on the TPV materials are transferred to stretch–stress responses as depicted in Figure 6 for the TPV ShA30 on the left (a) for the TPV ShA90 on the right side (b). Both tests are performed with specimens from plates produced with the parameter set MMM, meaning $T_C = 45°C$, $T_M = 208°C$, and $\dot{V} = 190\,cm^3/s$. Both graphs depict the previously mentioned load cycles applied to the specimen on three stretch levels. The differences in the mechanical response between the two materials are discussed in the following section. In Section 4.2, the effects of varying processing parameters on the mechanical response are investigated.

4.3.1 | Comparison of the two materials on characteristic properties

The resulting stress–stretch behaviors differ very significantly. The stiffness of the TPV ShA30 is more than one order of magnitude lower than that of the TPV ShA90.

15482634, 0, Downloaded from https://4spepublications.onlinelibrary.wiley.com/doi/10.1002/pen.26536 by Rwth Aachen Hochschulbibliothe, Wiley Online Library on [02/11/2023]. See the Terms and Conditions (https://onlinelibrary.wiley.com/terms-and-conditions) on Wiley Online Library for rules of use; OA articles are governed by the applicable Creative Commons License

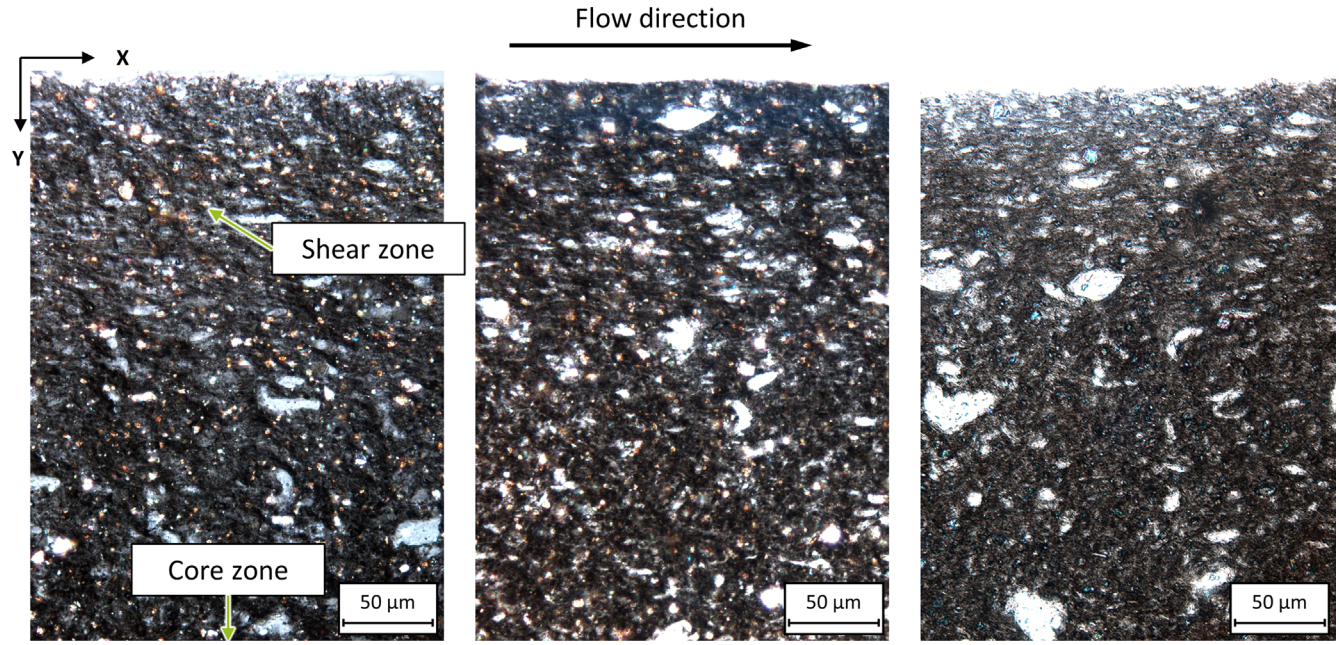


FIGURE 4 Higher resolution light microscopy images of the shear zone region of the TPV ShA90 for the most deviating machine parameter settings LLL (A), MMM (B), and HHH (C).

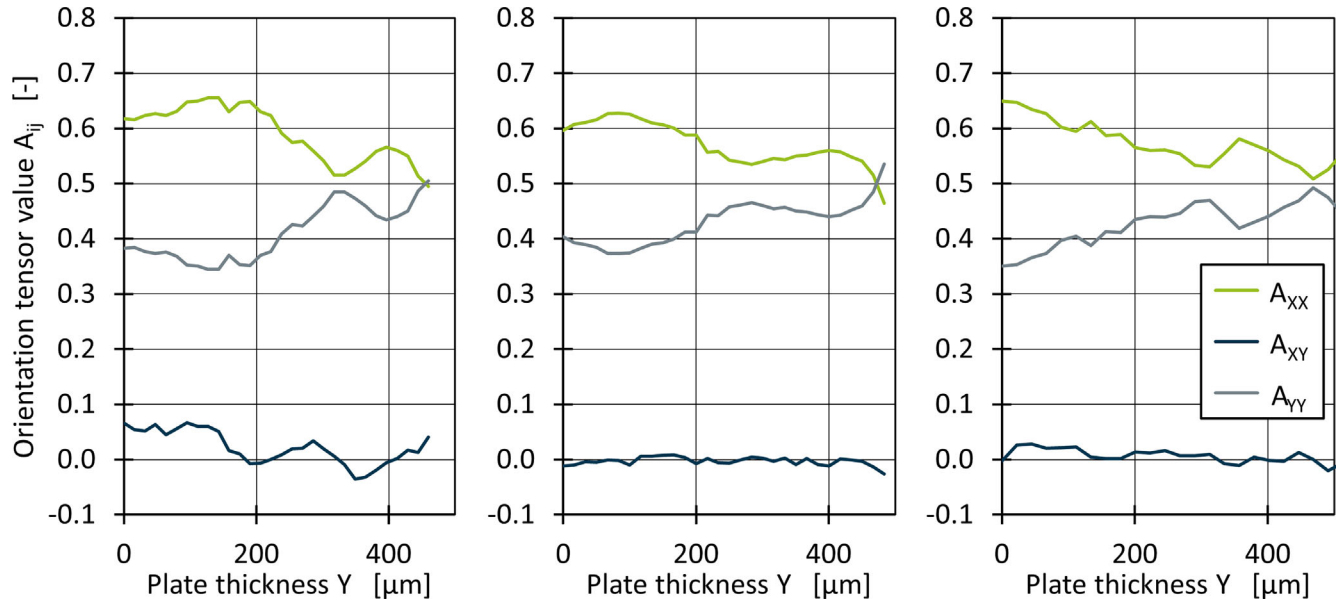


FIGURE 5 Rolling average particle orientation degree from microscopy images of the shear zone region of the TPV ShA90 for the machine parameter settings LLL (A), MMM (B), and HHH (C).

The average maximum stresses at $\lambda = 1.3$ are $\sigma = 0.35$ N/mm^2 for TPV ShA30 and 6.04 N/mm^2 for TPV ShA90. Also, the TPV ShA90 shows more significant signs of yielding at higher stretch levels compared with the much softer material. Both effects can be attributed to the higher content of PP in the TPV ShA90.[3] In addition, reduced effects of material deterioration due to the peroxidic cross-linking system and softening due to a lower amount of plasticizer may increase the stiffness of the TPV ShA90.[15,24]

The differences between the two material grades become much more evident when reducing the stress–stretch response to the first loading step of each stretch level. This observation can be interpreted as the stress–stretch response of the unstretched material since the curve approaches the virgin material stress response after

15482634, 0, Downloaded from https://4spepublications.onlinelibrary.wiley.com/doi/10.1002/pen.26536 by Rwth Aachen Hochschulbibliothe, Wiley Online Library on [02/11/2023]. See the Terms and Conditions (https://onlinelibrary.wiley.com/terms-and-conditions) on Wiley Online Library for rules of use; OA articles are governed by the applicable Creative Commons License

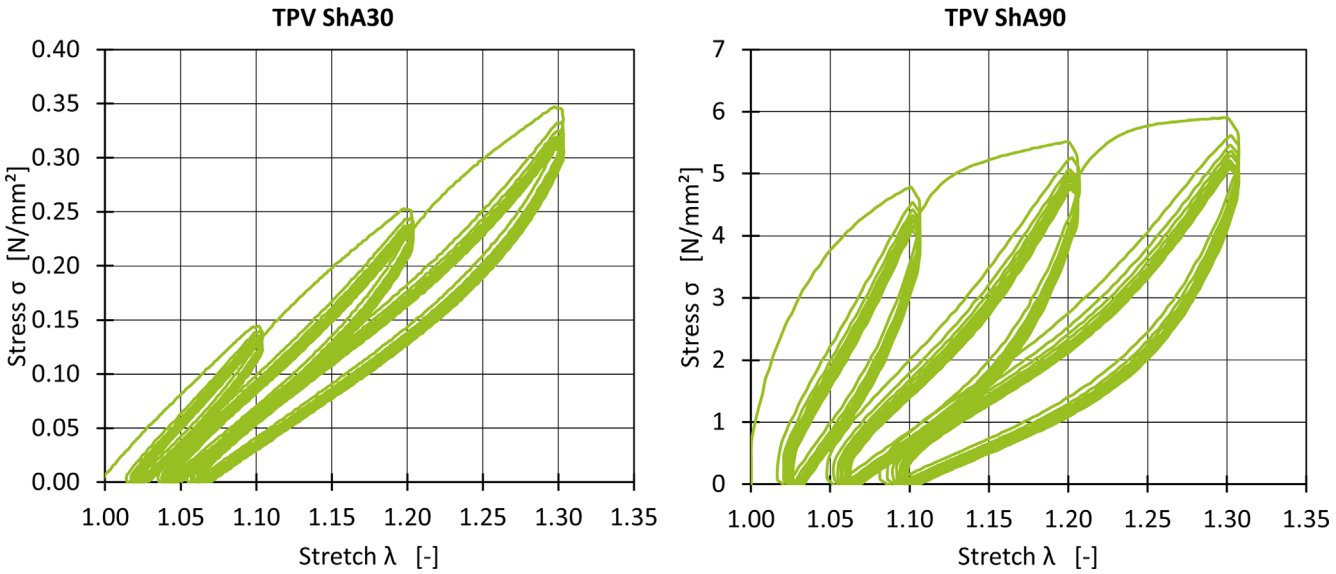


FIGURE 6 Stress–stretch curves for quasi-static cyclic uniaxial tension tests on (A) TPV ShA30 and (B) TPV ShA90 for the process parameter set MMM with an extraction orientation of 0°.

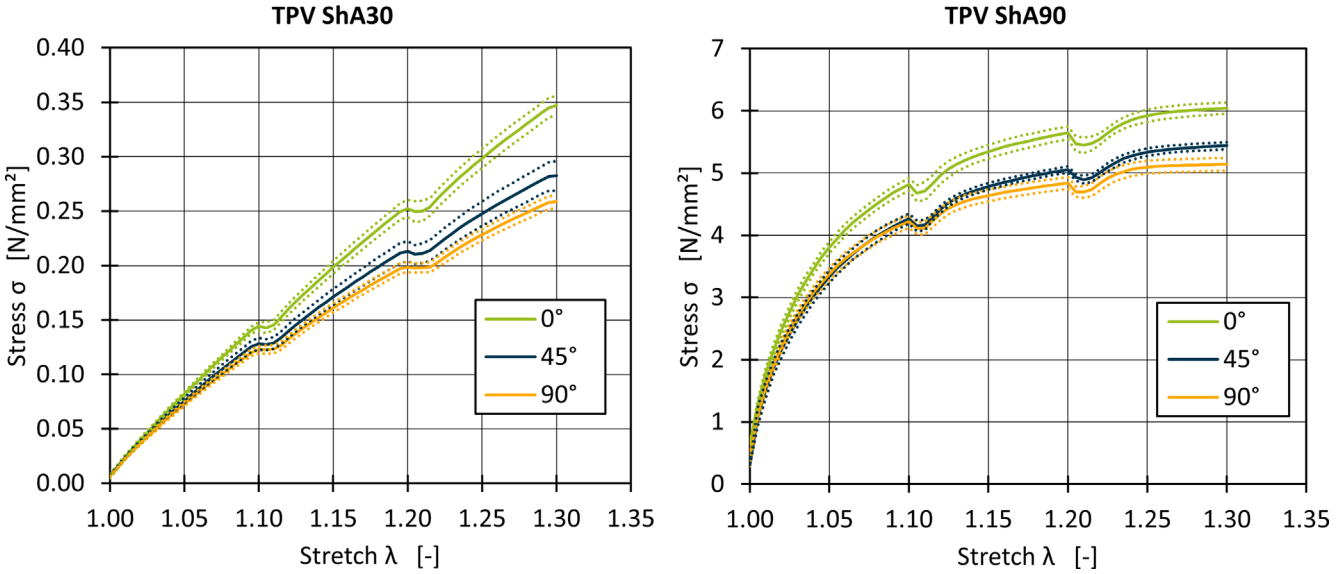


FIGURE 7 Reduced stress–stretch curves from uniaxial tension tests on (A) TPV ShA30 and (B) TPV ShA90 for the process parameter set MMM for three extraction orientations.

stretching the specimen further than the previous stretch level. With the reduction in displayed data, multiple plots for different extraction orientations can be plotted in the graphs. Hence, in Figure 7, the virgin stress–stretch curves are plotted for the three extraction orientations for each material. These solid curves represent the averaged material response from all tests. The dotted lines indicate the standard deviations from the individual tests.

In addition to that, the graphs in Figure 7 indicate the anisotropic behavior of both materials. They show decreasing stiffnesses with increasing specimen extraction angles. For quantification of the anisotropy of TPE, the anisotropy ratio R_A is introduced as the quotient of stress for 90° and 0° extraction orientation at equivalent stretch levels, with

$$R_A = 1 - \frac{\sigma_{90^\circ}(\lambda_i)}{\sigma_{0^\circ}(\lambda_i)}. \quad (5)$$

This value is plotted in dependence of the applied stretch in Figure 8 for both materials (TPV ShA30 [a] and TPV ShA90 [b]). In both cases, the anisotropy ratio continuously increases with increasing stretch after an initial transient phase. However, the incline for the TPV ShA90

15482634, 0, Downloaded from https://4spepublications.onlinelibrary.wiley.com/doi/10.1002/pen.26536 by Rwth Aachen Hochschulbibliothe, Wiley Online Library on [02/11/2023]. See the Terms and Conditions (https://onlinelibrary.wiley.com/terms-and-conditions) on Wiley Online Library for rules of use; OA articles are governed by the applicable Creative Commons License

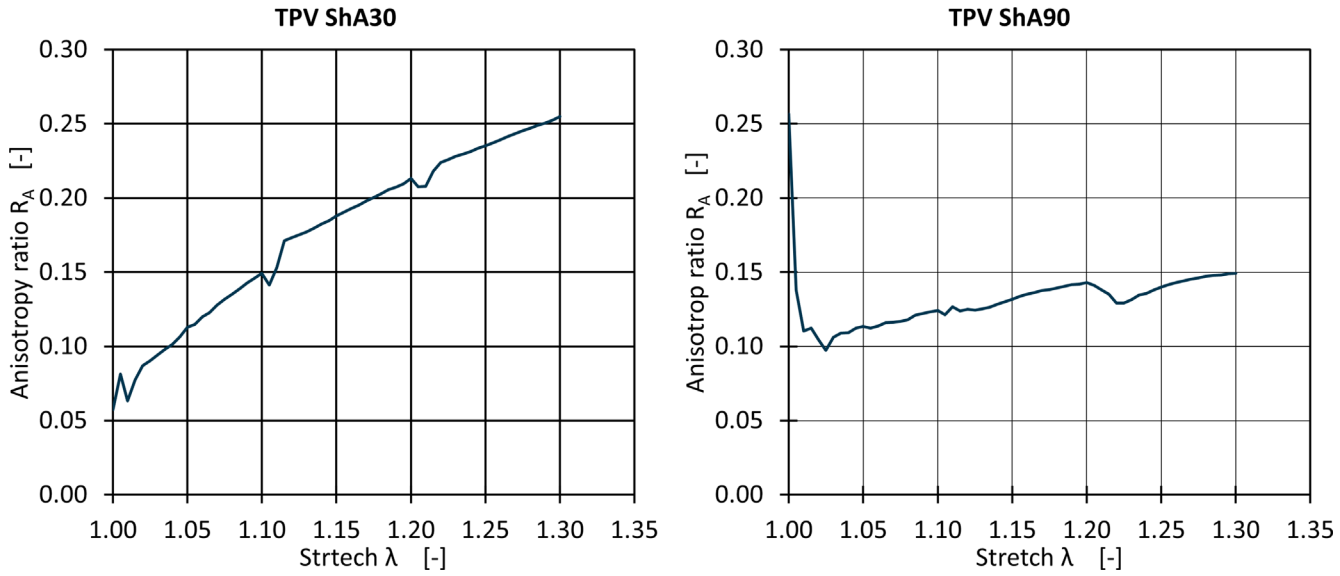


FIGURE 8 Anisotropy ratios of uniaxial tensile tests with 0° and 90° extraction orientation with respect to the applied stretch for (A) TPV ShA30 and (B) TPV ShA90 for the process parameter set MMM.

compound is significantly lower. Evaluating the anisotropy ratio, the TPV ShA compound initially shows higher anisotropy for lower stretch values. At $\lambda = 1.05$ and higher, the TPV ShA30 has a higher anisotropy for this processing configuration. In both cases, where the cyclic loading is applied at the stretch levels 1.1, 1.2, and 1.3, an indent in the curve is observed. After this indent, the curve usually approaches the previous trajectory. For the TPV ShA90 material, however, a clear discontinuity in the third load step ($\lambda = 1.3$) is found. It should be noted that through error propagation, the statistic variance of the anisotropy ratio is much higher than in the experimental stress–stretch response. The presented data are derived from the average stress–strain curves.

Finally, two other characteristic effects of the TPV materials are influenced by the elastomer content in the two compounds. These are the residual stretch after unloading in the tenth cycle and the reduction in maximum stress after 10 cycles. The residual stretch indicates the plastic deformation in the material. Though, it is not equivalent due to the viscoelastic potential that is still present directly after unloading. The stress reduction after cyclic loading indicates material damage equivalently to Mullins-damage in filled elastomer components. Both values are listed in Table 2 for the third stretch level of $\lambda = 1.3$.

Regarding the residual stretch after the tenth unloading step, the TPV ShA90 shows higher values with around $\lambda_{res} = 1{,}10$. The residual stretch in the TPV ShA30 is significantly lower with $\lambda_{res} = 1{,}06$. A significant dependence of the residual stretch on the extraction angle is not found. Similar effects are identified for stress reduction. The TPV ShA30 shows a lower stress reduction with $\sigma_{10}/\sigma_0 = 0.90$ in comparison with the TPV ShA90 with $\sigma_{10}/\sigma_0 = 0.87$. Here, also, an effect of the extraction angle is not identified. For the other stretch levels, similar results are found.

The influence of the processing parameters on the mechanical properties is investigated in detail in the following section. Nevertheless, the process parameter sets producing the extreme points in the mechanical response of the two investigated materials are presented here. Focusing on the stress response, the maximum stress at $\lambda = 1.3$ is compared between the reference parameter set MMM, and the sets producing maximum and minimum stress response for each material in Figure 9.

The parameter set LLL results in the highest stress response for both materials. It is worth mentioning that, for the TPV ShA30, this parameter set produces the highest maximum stresses in all extraction orientations. Other anisotropic materials, such as short-fiber composites, would be expected to show a different effect due to phase morphology alone. A stronger orientation would result in a higher stress response in that direction. Perpendicular to that, however, the stress response should be reduced.[25,26] This behavior indicates that not only the phase morphology is changed by the processing parameters. Further influences can be the crystallization of the PP phase or the chemical deterioration of the PP phase due to the peroxidic cross-linking agent during processing. The parameter set LLL has the lowest processing temperatures. Hence, the process of chemical deterioration is much slower. This would explain the higher stiffnesses for this parameter set.

In order to investigate the influence of the processing parameters on the anisotropy of the material, the anisotropy ratios for the three stretch levels at maximum stress are depicted in Figure 10 (a) for the TPV ShA30 and

15482634, 0, Downloaded from https://4spepublications.onlinelibrary.wiley.com/doi/10.1002/pen.26536 by Rwth Aachen Hochschulbibliothek, Wiley Online Library on [02/11/2023]. See the Terms and Conditions (https://onlinelibrary.wiley.com/terms-and-conditions) on Wiley Online Library for rules of use; OA articles are governed by the applicable Creative Commons License

Material	Extraction orientation	Residual stretch λ_{res} Avg.	Residual stretch λ_{res} Std. dev.	Stress reduction σ_{10}/σ_0 Avg.	Stress reduction σ_{10}/σ_0 Std. dev.
TPV ShA30	0°	1.060	0.003	0.894	0.008
	45°	1.062	0.003	0.911	0.004
	90°	1.064	0.004	0.909	0.003
TPV ShA90	0°	1.107	0.007	0.864	0.005
	45°	1.111	0.005	0.865	0.007
	90°	1.112	0.008	0.875	0.012

TABLE 2 Average (Avg.) and standard deviation (Std. dev.) of residual stretch and reduction in the maximum stretch after 10 loading cycles on the third stretch level ($\lambda = 1.3$) in dependence on the material and extraction orientation for the process parameter set MMM.

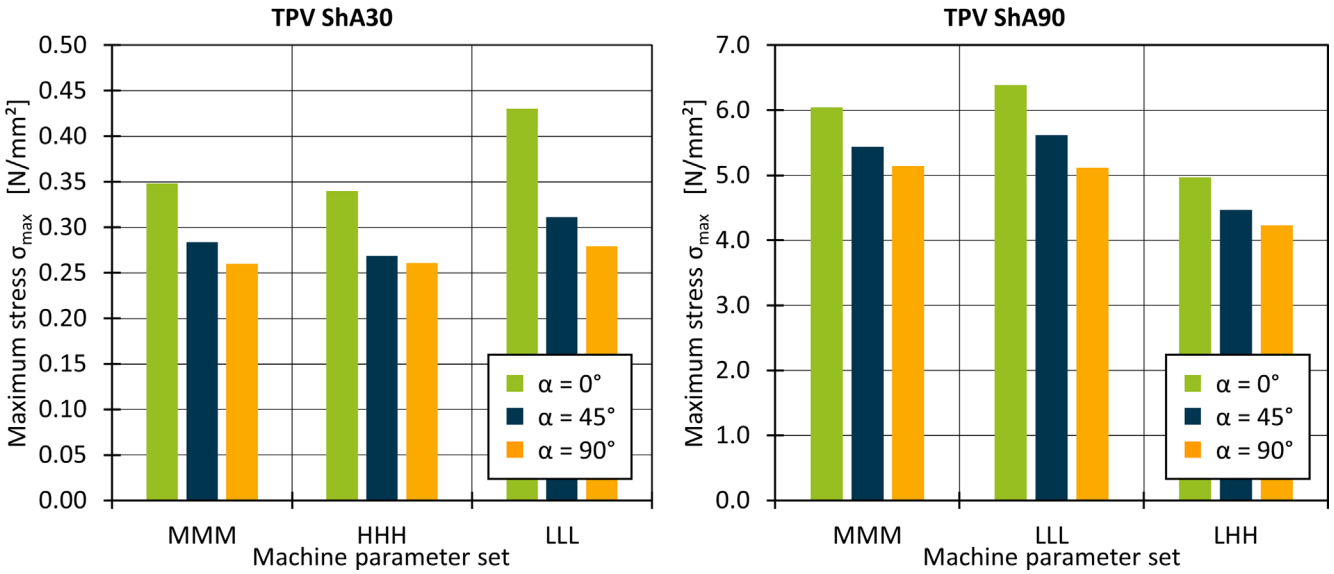


FIGURE 9 Maximum stress at $\lambda = 1.3$ from uniaxial tension tests for the process parameter sets producing the maximum and minimum stress response for the (A) TPV ShA30 and (B) TPV ShA90 materials compared with the reference production parameter set MMM.

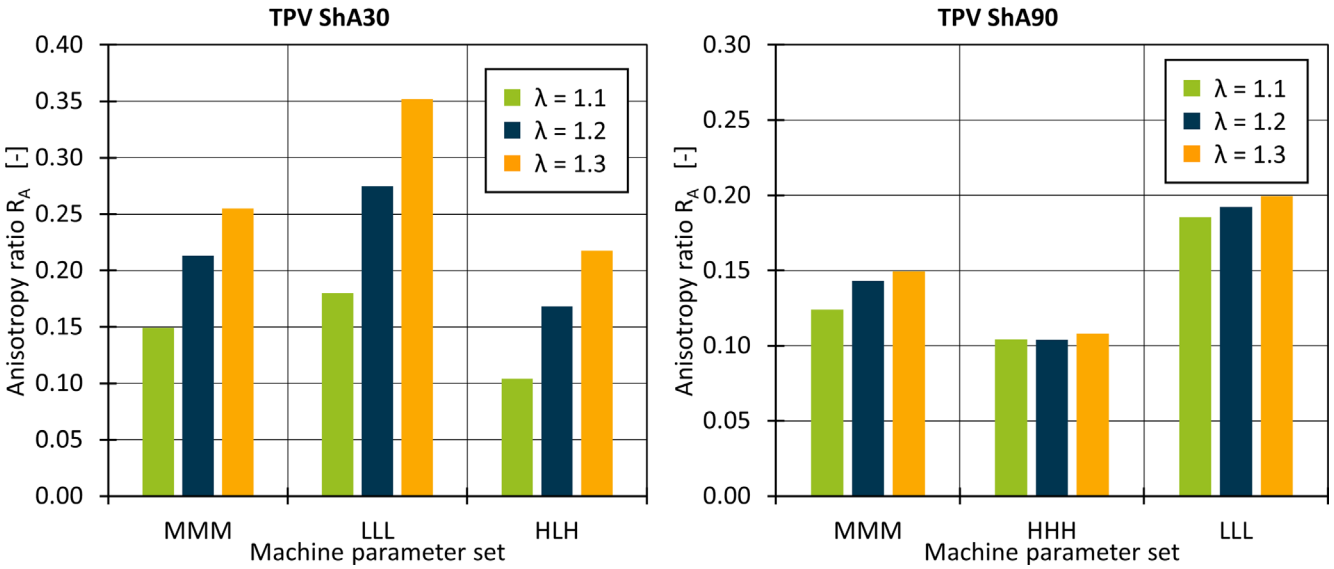


FIGURE 10 Anisotropy ratios from uniaxial tension tests at different stretch levels for the process parameter sets producing the maximum and minimum values for the (A) TPV ShA30 and (B) TPV ShA90 materials compared with the reference production parameter set MMM.

15482634, 0, Downloaded from https://4spepublications.onlinelibrary.wiley.com/doi/10.1002/pen.26536 by Rwth Aachen Hochschulbibliothe, Wiley Online Library on [02/11/2023]. See the Terms and Conditions (https://onlinelibrary.wiley.com/terms-and-conditions) on Wiley Online Library for rules of use; OA articles are governed by the applicable Creative Commons License

(b) for the TPV ShA90. Again, the processing parameter sets that result in the extreme values for anisotropy are chosen here and compared with the reference parameter set MMM. In analogy to the maximum stress response, the parameter set LLL produces the highest anisotropy ratios for both materials. The lowest anisotropy is found at the process parameter sets HLH for the TPV ShA30 and HHH for the TPV ShA90. Worth mentioning is that a lower injection speed leads to higher anisotropy in this case. This seems counterintuitive since higher injection speeds should result in higher shear rates in the cavity and, consequently, higher particle distortion. Following this theory, the process parameter set LLH should result in higher anisotropies than LLL. One explanation for the inverse effect, which was observed here, could be the shear heating effects. Due to the higher injection speeds, the melt is warmer, and the PP-phase takes longer to freeze. This allows the elastomer particles to recover from their deformations before the matrix material and, thus, the inclusion deformation is frozen.

4.3.2 | Influence of processing machine settings on the anisotropy of the material

In this section, the influence of the processing machine settings on the characteristic material properties of TPV is investigated in more detail. Especially an effect analysis is conducted on the three varied processing parameters: cavity temperature, melt temperature, and injection volume flow, and their coupled effects from the fully factorial test plan, defined in Section 3.2. The previous section already demonstrated the complex effects of the processing and their interactions on the mechanical properties of TPV. Most significant effects are identified in the maximum stress response and the anisotropy factor. Hence, the influence of the processing on these properties is investigated.

To examine the effects on the overall shift of the maximum stress response, the influence of anisotropy is initially neglected. Therefore, a comparative stress response is introduced by the average of the maximum stresses at 0° and 90° extraction orientation. The effects of the processing parameters and their coupled effects are depicted in Figure 11A,B for the TPV ShA30 and the TPV ShA90 materials, respectively. The effects are normalized by the average stress response overall process parameter sets for better comparison between the two materials. The solid, dashed, and dotted lines depict the confidence intervals for 95%, 99%, and 99.9% confidence levels, respectively.

For both materials, it is observed that the direct effects of the processing parameters significantly influence the maximum stress response. For the coupled effects, only the coupling of the cavity and melt temperature seem to influence the maximum stress significantly in a synergetic manner. Comparing the two materials, the opposite effect of the cavity temperature on the maximum stress is initially noticed. Both effects are found to be significant, with a confidence level of more than 99.9%. For the TPV ShA30 material, the cavity

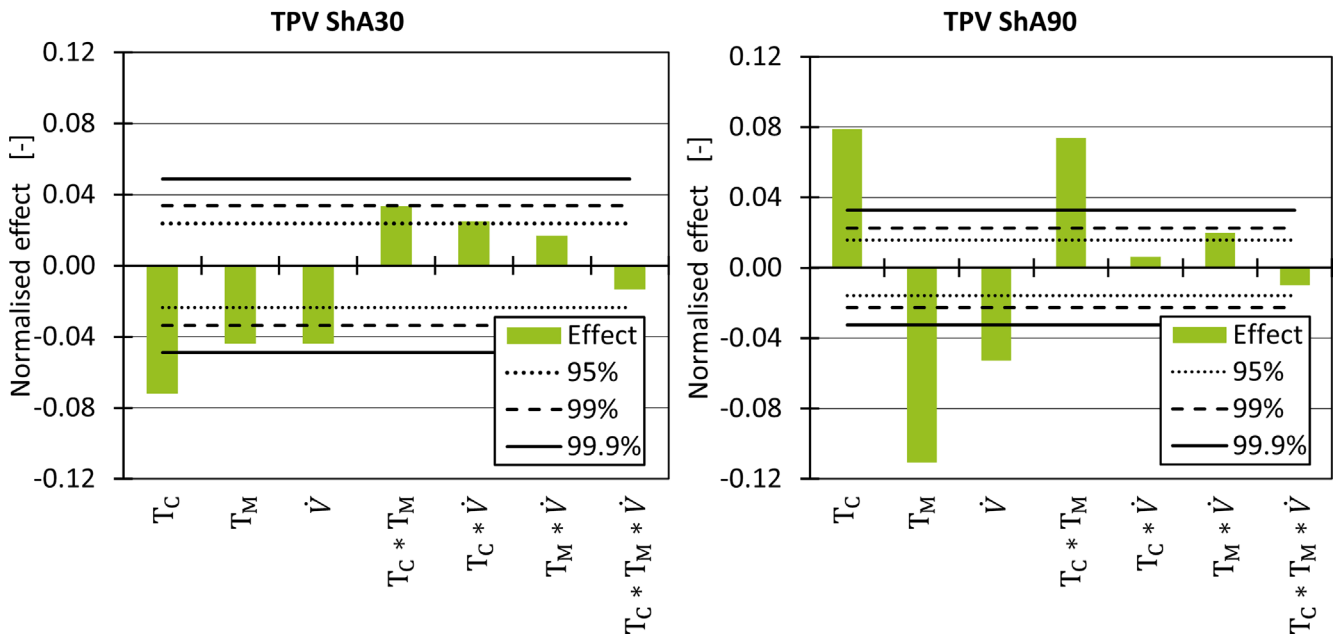


FIGURE 11 Effects and coupled effects of processing parameters on the comparative maximum stress response for the (A) TPV ShA30 and (B) TPV ShA90 materials.

15482634, 0, Downloaded from https://4spepublications.onlinelibrary.wiley.com/doi/10.1002/pen.26536 by Rwth Aachen Hochschulbibliothe, Wiley Online Library on [02/11/2023]. See the Terms and Conditions (https://onlinelibrary.wiley.com/terms-and-conditions) on Wiley Online Library for rules of use; OA articles are governed by the applicable Creative Commons License

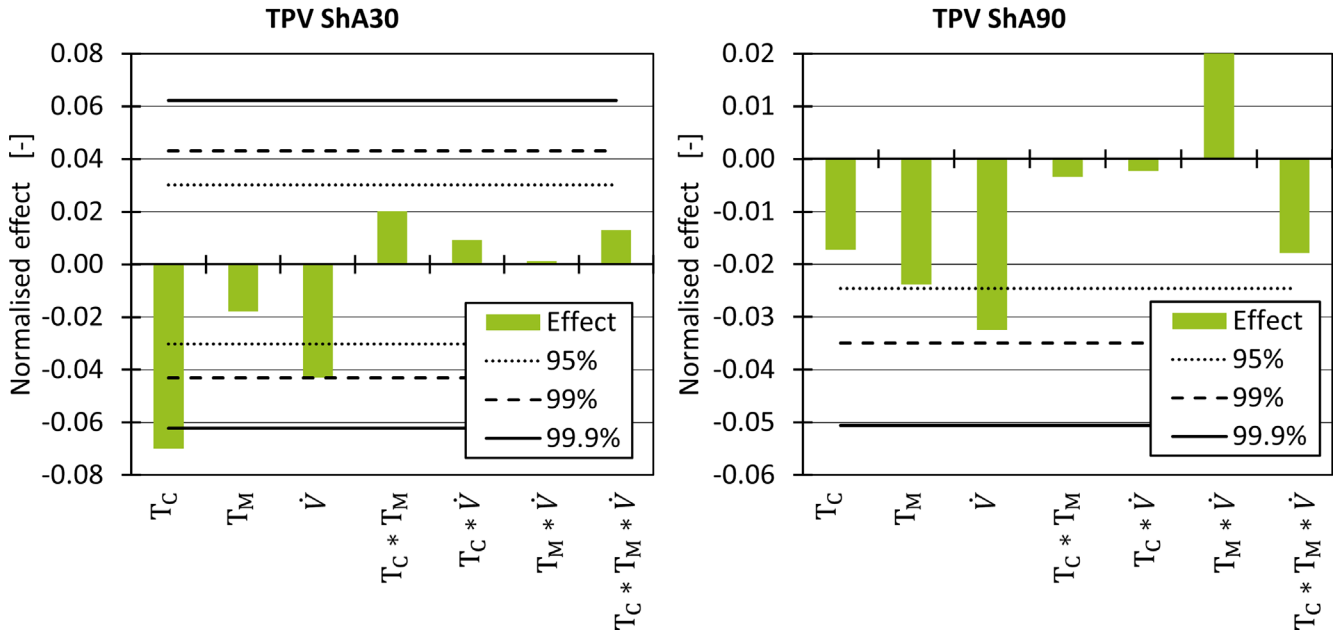


FIGURE 12 Effects and coupled effects of processing parameters on the anisotropy ratio for the (A) TPV ShA30 and (B) TPV ShA90 materials.

temperature is found to have the highest absolute effect on the maximum stress response. The most considerable absolute effect for the TPV ShA90 material is found with the melt temperature T_M. The effect is negative, meaning that an increased melt temperature would result in a reduced maximum stress response. This could be attributed to the loss of material stiffness in the thermoplastic component due to the chemical deterioration from the peroxidic crosslinking agent. The change of thermoplastic properties would also explain the smaller effect on the TPV ShA30 material since a lower thermoplastic content is present. Additionally, the TPV ShA90 material is at this stretch state already subject to extensive yielding, whereas the TPV ShA30 is still primarily elastic. Finally, the negative effect of the injection volume flow rate on the maximum stress response is observed. This effect is already described in Section 4.2 and attributed to the increased shear heating effects and, hence, longer relaxation time for the elastomer particles.

Figure 12 depicts the effect analysis of the process parameter variation on the anisotropy of the materials. Again, in (a), the effects for the TPV ShA30 and, in (b), the effects for the TPV ShA90 are visualized. Since the anisotropy factor is already a normalized value, these effect values are not normalized. It is observed that all three main factors of the test plan have a negative effect on the anisotropy for both materials. For the TPV ShA90, however, only the effect of the injection flow rate exceeds the 95% confidence interval. For the TPV ShA30 material, this is the case for the cavity temperature and the volume flow rate. Coupled effects are not found significant for both materials. Hence, the obtained effects are interpreted to be superpositional. However, the melt temperature and volume flow coupling are just below the 95% confidence interval for the TPV ShA90. Negative effects of cavity and melt temperatures result from the reduced viscosity of the melt and the longer relaxation period of the elastomer particles. The negative effect of the injection flow rate may also be explained by higher melt temperatures due to shear heating during the injection. Similar effects have been observed in Reference 3.

5 | DISCUSSION

Comparing the results from the microscopy images with the mechanical investigations, many correlations can be found. First, it seems plausible that a higher orientation state in the elastomer particles results in a higher anisotropy of the material. This is primarily supported by the through-thickness investigation of the orientation state of the TPV ShA90. Higher orientation degrees can be expected for the softer TPV ShA30 due to the higher amount of elastomer particles and the observed higher anisotropy in the material. However, microscopy images cannot be provided at this point due to the natural coloring of the compound, which does not allow for the inclusion detection from contrasting. Additionally, the specimen preparation of the TPV ShA30 demands special cutting tools and low ambient temperatures, which could not be achieved with the microtome used in these investigations.

15482634, 0, Downloaded from https://4spepublications.onlinelibrary.wiley.com/doi/10.1002/pen.26536 by Rwth Aachen Hochschulbibliothe, Wiley Online Library on [02/11/2023]. See the Terms and Conditions (https://onlinelibrary.wiley.com/terms-and-conditions) on Wiley Online Library for rules of use; OA articles are governed by the applicable Creative Commons License

Secondly, the process parameters have a counterintuitive influence on the local orientation state in the compound. Opposite to other materials with process-induced anisotropy, such as short fiber-reinforced composites, increasing shear rates within the melt do not result in higher anisotropy and elastomer particle distortion. This is indicated by the strong negative effect of injection speed on the anisotropy of the TPV. Usually, higher shear rates would result in higher distortion and orientation of the particles and, consequently, higher local anisotropy. A possible explanation of the inverse effect comes from the self-heating of the melt resulting from the shear flow. Increasing temperature in the melt increases the cooling time in the process additionally, so the viscoelastic retraction of the elastomer particles is supported by the lower viscosity of the melt. Another effect could be the rupture of elastomer particles during the injection molding process reducing particle deformation. However, the microscopy images do not show any qualitative signs of reduced particle size for higher orientation states. Further investigations must be taken to understand the ongoing processes better. It should also be noted that the other investigated factors, namely cavity and melt temperature, have a similar effect on the anisotropy as observed for short-fiber composites.

Subsequently, the observed significant impact of the machine parameter settings on the maximum stress must be further discussed. It cannot be explained by local morphology effects. One explanation is the chemical decomposition of the thermoplastic phase due to the presence of active peroxidic cross-linking agents. This explanation is supported by the strong effects of higher melt temperature, especially for the TPV ShA90. A reduction in stiffness of the polypropylene phase due to the chemical decomposition could additionally result in a reduction of the local anisotropy. Micro-mechanical investigations have shown that the anisotropy is primarily related to the thin thermoplastic regions between two elastomer particles.[27] Further investigations on the chemical decomposition of the material are necessary.

6 | CONCLUSIONS

The influence of the injection molding process settings on the local phase morphology and mechanical properties of TPV has been investigated. Significant effects of the machine parameters melt, cavity temperature, and injection volume flow rate on the macroscopic anisotropy have been observed. The effect of the injection flow rate is found to be inverse to the expected. From other anisotropic materials, a positive effect of the volume flow rate on the anisotropy ratio would be expected. However, for TPV, a significant negative effect is found and can also be confirmed by the microscopic investigations of the phase morphology. Higher injection speeds result in lower particle deformation and a lower thickness of the shear zone with highly distorted particles. During the process, it is assumed that the self-heating of the melt causes the elastomer particles to experience longer relaxation times before the thermoplastic matrix is consolidated. Another important observation is the significant effect of the machine settings on the resulting maximum stress response at 30% strain. This influence is attributed to the chemical decomposition of the polypropylene matrix polymer chains due to the presence of active peroxidic cross-linking systems. Here, contradicting significant effects have been found for the two investigated materials for the cavity temperature factor. This may be attributed to the different amounts of PP. The relation to the chemical decomposition of the PP phase has to be confirmed by chemical analyses of the injection molded material.

AUTHOR CONTRIBUTIONS

Noah Mentges contributed to conceptualization, methodology, software, validation, formal analysis, investigation, resources, data curation, writing – original draft, visualization. Hakan Çelik contributed to conceptualization, methodology, formal analysis, writing – review and editing, supervision. Rainer Dahlmann contributed to writing – review and editing, supervision, funding acquisition. Christian Hopmann contributed to writing – review and edition, supervision, project administration, funding acquisition. All authors have read and agreed to the published version of the manuscript.

ACKNOWLEDGMENTS

The material for the macroscopic mechanical tests and microscopic investigations was provided by the MOCOM Compounds GmbH & Co. KG, Hamburg, Germany. We would like to express our gratitude for this. Open Access funding enabled and organized by Projekt DEAL.

FUNDING INFORMATION

This research was funded by German Research Foundation (DFG), grant number 448100263. We would like to extend our thanks to the DFG.

CONFLICT OF INTEREST STATEMENT

The authors declare that they have no conflict of interest. The funders had no role in the design of the study, in the collection, analyses, or interpretation of data; in the writing of the manuscript; or in the decision to publish the results.

DATA AVAILABILITY STATEMENT

The data that support the findings of this study are available from the corresponding author upon reasonable request.

15482634, 0, Downloaded from https://4spepublications.onlinelibrary.wiley.com/doi/10.1002/pen.26536 by Rwth Aachen Hochschulbibliothe, Wiley Online Library on [02/11/2023]. See the Terms and Conditions (https://onlinelibrary.wiley.com/terms-and-conditions) on Wiley Online Library for rules of use; OA articles are governed by the applicable Creative Commons License

ORCID

Noah Mentges https://orcid.org/0000-0002-2539-2624
Hakan Çelik https://orcid.org/0000-0001-6851-7063

REFERENCES

1. Boyce MC, Socrate S, Kear K, Yeoh OH, Shaw K. Micromechanisms of deformation and recovery in thermoplastic vulcanizates. *J Mech Phys Solids*. 2001;49(6):1323-1342.
2. Asami T, Nitta K. Morphology and mechanical properties of polyolefinic thermoplastic elastomer I. Characterization of deformation process. *Polymer*. 2004;45(15):5301-5306.
3. Hopmann C, Bruns P, Schöngart M. Influence of the injection molding process on the morphology of thermoplastic vulcanizates. In: Proceedings of the regional conference Graz 2015 - Polymer Processing Society: PPS Conference papers. Vol 1779. 2016:80013.
4. Michaeli W, Masberg U, Hopmann C, Köppen H, Dering JP. Gezielte Beeinflussung der Materialeigenschaften von thermoplastischen Vulkanisaten in Kautschukinnenmischern. *KGK Rubberpoint*. 2011;9:26-32.
5. Abdou-Sabet S, Puydak RC, Rader CP. Dynamically vulcanized thermoplastic elastomers. *Rubber Chem Technol*. 1996;69(3):476-494.
6. Boyce MC, Kear K, Socrate S, Shaw K. Deformation of thermoplastic vulcanizates. *J Mech Phys Solids*. 2001;49(5):1073-1098.
7. Boyce MC, Yeoh OH, Socrate S, Kear K, Shaw K. Micromechanics of cyclic softening in thermoplastic vulcanizates. *J Mech Phys Solids*. 2001;49(6):1343-1360.
8. Bhattacharya AB, Raju AT, Chatterjee T, Naskar K. Development and characterizations of ultra-high molecular weight EPDM/PP based TPV nanocomposites for automotive applications. *Polym Compos*. 2020;41(12):4950-4962.
9. Zohrevand A, Goharpey F, Nasrollah Gavgani J, Foudazi R. The effect of aggregation of cured rubber particles on rheology of thermoplastic vulcanizates. *Polym Compos*. 2020;41(4):1376-1392.
10. Hopmann C, Zimmermann C. Characterisation of the quasi-static material behaviour of thermoplastic elastomers (TPE) under consideration of temperature and stress state. *J Elastomers Plast*. 2020;52(3):199-215.
11. Hopmann C, Mentges N, Zimmermann C, Dahlmann R. Simulative implementation of the influence of the load direction on the long-term behaviour of thermoplastic elastomers, in DKT IRC 2021 (Ed Deutsche Kautschuk Gesellschaft e. V.), 27.06.2022, Nuremberg, Germany. 2022.
12. Burgoa A, Arriaga A, Badiola JH, et al. On the injection molding of thick-walled thermoplastic vulcanizates: linking static and dynamic mechanical properties with morphology. *Polymer* International. 2023;72:508-519.
13. Oderkerk J, Groeninckx G, Soliman M. Investigation of the deformation and recovery behavior of Nylon-6/rubber thermoplastic Vulcanizates on the molecular level by infrared-strain recovery measurements. *Macromolecules*. 2002;35(10):3946-3954.
14. Soliman M, van Dijk M, van Es M, Shulmeister V. Deformation Mechanism of Thermoplastic Vulcanizates Investigated by Combined FTIR – and Stress-Strain Measurements, in *ANTEC 1998* (ed SPE), p. 86. 1998.
15. Kurzidim F. *Prozess und Materialeigenschaften bei der Herstellung von thermoplastischen Vulkanisaten im Zweischneckenextruder*. Martin-Luther-Universität; 2014 Dissertation.
16. Stanic S, Koch T, Schmid K, Knaus S, Archodoulaki V-M. Upcycling of polypropylene with various concentrations of peroxydicarbonate and dilauroyl peroxide and two processing steps. *J Appl Polym Sci*. 2021;138(28):50659.
17. Mocom Compounds GmbH & Co. KG. Technical Data Sheet: Alfater XL A30I 4GP0000. 2020.
18. Mocom Compounds GmbH & Co. KG. Technical Data Sheet: Alfater XL A90I 4GP0000. 2020.
19. 53504. Prüfung von Kautschuk und Elastomeren, Deutsches Institut für Normung e. V., Berlin. 2017.
20. Otsu N. A threshold selection method from gray-level histograms. *IEEE Trans Syst Man Cybern*. 1979;9(1):62-66.
21. Advani SG, Tucker CL III. The use of tensors to describe and predict fiber orientation in short fiber composites. *J Rheol*. 1987;31(8):751-784.
22. Basser PJ, Pierpaoli C. Microstructural and physiological features of tissues elucidated by quantitative-diffusion-tensor MRI. *J Magn Reson B*. 1996;111(3):209-219.
23. Folgar F, Tucker CL III. Orientation behavior of fibers in concentrated suspensions. *J Reinf Plast Compos*. 1984;3(2):98-119.
24. Naskar K. *Dynamically Vulcanized PP/EPDM Thermoplastic Elastomers: Exploring Novel Routes for Crosslinking with Peroxides*. University of Twente; 2004 Dissertation.
25. Mentges N, Dashtbozorg B, Mirkhalaf SM. A micromechanics-based artificial neural networks model for elastic properties of short fiber composites. *Compos Part B Eng*. 2021;213:108736.
26. Mentges N, Çelik H, Hopmann C, Fagerström M, Mirkhalaf SM. Micromechanical modelling of short fibre composites considering fibre length distributions. *Compos Part B Eng*. 2023;264:110868.
27. Mentges N, Çelik H, Dahlmann R, Hopmann C. Modelling the effects of process induced phase morphology on the mechanical response of thermoplastic vulcanisates under quasi-static loading using representative volume elements, in *IRC RubberCon*. IRC Rubber con, Edinburgh, United Kongdom, Edinburgh, UK. 2023.

SUPPORTING INFORMATION

Additional supporting information can be found online in the Supporting Information section at the end of this article.

How to cite this article: Mentges N, Çelik H, Dahlmann R, Hopmann C. Effects of the injection molding processing settings on the phase morphology and mechanical anisotropy of thermoplastic vulcanizates. *Polym Eng Sci*. 2023; 1-16. doi:10.1002/pen.26536

15482634, 0, Downloaded from https://4spepublications.onlinelibrary.wiley.com/doi/10.1002/pen.26536 by Rwth Aachen Hochschulbibliothe, Wiley Online Library on [02/11/2023]. See the Terms and Conditions (https://onlinelibrary.wiley.com/terms-and-conditions) on Wiley Online Library for rules of use; OA articles are governed by the applicable Creative Commons License